Synthesis, thermal stability and magnetic properties of an interpenetrated Mn(II) triazolate coordination framework

Richard Röß-Ohlenroth, Marcel Hirrle, Maryana Kraft, Andreas Kalytta-Mewes, Anton Jesche, Hans-Albrecht Krug von Nidda, Dirk Volkmer

Angaben zur Veröffentlichung / Publication details:

Röß-Ohlenroth, Richard, Marcel Hirrle, Maryana Kraft, Andreas Kalytta-Mewes, Anton Jesche, Hans-Albrecht Krug von Nidda, and Dirk Volkmer. 2022. "Synthesis, thermal stability and magnetic properties of an interpenetrated Mn(II) triazolate coordination framework." *Zeitschrift für anorganische und allgemeine Chemie* 648 (16): e202200153. https://doi.org/10.1002/zaac.202200153.

Journal of Inorganic and General Chemistry
ZAAC
Zeitschrift für anorganische und allgemeine Chemie
www.zaac.wiley-vch.de
RESEARCH ARTICLE
DOI: 10.1002/zaac.202200153

Synthesis, Thermal Stability and Magnetic Properties of an Interpenetrated Mn(II) Triazolate Coordination Framework

Richard Röß-Ohlenroth,[a] Marcel Hirrle,[a] Maryana Kraft,[a] Andreas Kalytta-Mewes,[a] Anton Jesche,[b] Hans-Albrecht Krug von Nidda,[c] and Dirk Volkmer*[a]

Coordination frameworks and metal-organic frameworks built from simple triazole ligands such as 1*H*-1,2,3-triazole (**H-ta**) have recently inspired great interest owing to physical phenomena such as electronic conductivity, phase transitions and their magnetic behavior. In line of our endeavors we report on the solvothermal reaction of $MnCl_2 \cdot 4H_2O$ with **H-ta** ligand in isopropyl alcohol leading to the the novel **CFA-23** (((propan-2-yl)oxidanium)$^+$[$Mn_6Cl_5(ta)_8$]$^-$; CFA-23 = Coordination Framework Augsburg University-23) coordination framework. Single-crystal X-ray diffraction (SC-XRD) reveals that it crystallizes in the tetragonal space group $P4_2/nnm$ (134) exhibiting a two-fold interpenetrated framework with the topologies of a ***dia*** net with point (Schläfli) symbol 6^6. The thermal stability of this compound was investigated using variable temperature X-ray powder diffraction and thermogravimetric analysis. The magnetic properties of **CFA-23** differ from a similar non-interpenetrated literature structure of the composition (H-[$Mn_6(bta)_8Cl_5$]$\cdot(H_2O)_4$) built from 1*H*-1,2,3-benzotriazole, thus, indicating that sterically induced lattice changes might be an adjustment parameter for magnetic properties in such frameworks.

Introduction

1,2,3-Triazolate based coordination compounds and especially metal-organic frameworks (MOFs) recently gained increasing attention owing to various physical phenomena and potential applications like e.g. drug delivery,[1] catalytic reactions,[2] kinetic trapping of gases,[3,4] H_2/D_2 quantum sieving[5] and CO_2 binding,[6] which were shown for bistriazolate MOFs featuring Kuratowski-type secondary building units (SBUs). Other bistriazolate-based frameworks were investigated for catalysis,[7] gas binding,[8–10] chirality,[11] magnetic behaviour,[12] or even electrical and proton conductivity.[13,14] Single triazolate ligands tend to form Kuratowski complexes,[15] which were recently proven to give interesting chromophores[16] or building blocks for the assembly of metal hydrogen-bonded organic frameworks[17] via functionalization of the ligand backbones. However, the 1*H*-1,2,3-triazole (**H-ta**) tends to form MOFs of the $M^{II}(ta)_2$-type,[18–20] which can be considered as a framework of condensed Kuratowski units. Such frameworks exhibit a variety of fascinating physical phenomena like e.g. Jahn-Teller and spin-crossover phase transitions,[19,21] electronic conductivity,[13,18,22] and even the highest ferromagnetic ordering temperature achieved in MOFs so far.[23] **H-ta** based frameworks built from Mn(II) ions are also promising materials for magnetic investigations due to their half-filled d-shell.[24] In literature, various structures built from Mn_4Cl SBUs with tetrazolate ligands are known.[25,26] However, to the best of our knowledge, only a MOF comprising Co_4Cl tetranuclear SBUs was investigated for its magnetic behavior[27] and DFT + D2 calculations of M_4Cl (M = Ti^{II}, V^{II}, Cr^{II}, Mn^{II}, Fe^{II}, Ni^{II}, Cu^{II}) SBUs also indicate antiferromagnetic ordering.[28] As long distances prevent the magnetic interaction between SBUs in most MOFs,[29] the coupling between the isolated Mn_4Cl SBUs can be enhanced by linkage via additional metal sites similar to the $M(ta)_2$ frameworks, as exemplified with the spin-canted MOF of the composition H-[$Mn_6(bta)_8Cl_5$]$\cdot(H_2O)_4$.[30]

In the effort to extend the variety of structures and our knowledge on the foundation of physical phenomena in such compounds, we synthesized and characterized the **CFA-23** (((propan-2-yl)oxidanium)$^+$ [$Mn_6Cl_5(ta)_8$]$^-$) framework. Particular emphasis is put on structural and magnetic properties in comparison to the related H[$Mn_6(bta)_8Cl_5$]$\cdot(H_2O)_4$ MOF. The structure was solved using single-crystal X-ray diffraction (SC-

[a] R. Röß-Ohlenroth, M. Hirrle, Dr. M. Kraft, A. Kalytta-Mewes, Prof. Dr. D. Volkmer
Universität Augsburg, Institut für Physik
Lehrstuhl für Festkörperchemie
Universitätsstraße 1, 86159
Augsburg (Germany)
E-mail: dirk.volkmer@physik.uni-augsburg.de
[b] Dr. A. Jesche
Universität Augsburg, Institut für Physik
Zentrum für Elektronische Korrelationen und Magnetismus,
Experimentalphysik VI,
Universitätsstraße 1, 86159
Augsburg (Germany)
[c] H.-A. Krug von Nidda
Universität Augsburg, Institut für Physik
Zentrum für Elektronische Korrelationen und Magnetismus,
Experimentalphysik V,
Universitätsstraße 1, 86159
Augsburg (Germany)

Supporting information for this article is available on the WWW under https://doi.org/10.1002/zaac.202200153

XRD), revealing a two-fold interpenetrated framework which can be ascribed to the missing benzene rings of the **H-ta** ligand when compared to the analogous framework containing benzotriazolate linkers. The 2-fold interpenetration leads to ultra-narrow channels extending along the *c*-direction of the framework. The framework's stability was investigated by variable temperature powder X-ray diffraction (VT-PXRD), as well as thermogravimetric analysis coupled with mass spectrometry (TGA-MS). In addition, we demonstrate that the molar magnetic susceptibility of the compound can be reasonably approximated using minimalistic models of the exchange interactions.

Results and Discussion

Synthesis

The novel **CFA-23** structure was discovered during reaction condition screening experiments similar to the $Mn(ta)_2$ single crystal syntheses described in literature.[31] Hereby, **CFA-23** was obtained using teflon lined steel autoclaves (23 mL inner volume) for solvothermal reaction conditions with a 1:2 metal-to-ligand ratio in isopropyl alcohol at 210 °C. During these investigations we noticed that the usage of new teflon liners is essential, as older vessels tended to give mixed phases with an unidentified impurity. Upscaling attempts employing 200 mL inner volume autoclaves were also unsuccessful so far, indicating a narrow window for the appropriate synthesis conditions. Thus, we deduce that formation of **CFA-23** might be mainly, but not exclusively, sensitive to the reaction pressure and temperature ramp, which differs for reaction vessels with largely different volumes.

Crystal Structure and Topology

SC-XRD revealed that **CFA-23** crystallizes in the tetragonal space group $P4_2/nnm$ (134) with unit cell dimensions of $a = b =$ 14.4426(4) Å and $c = 10.2366(3)$ Å (Table 1). Analysis with the ToposPro software package[32] revealed a two-fold interpenetration of the ***dia*** nets with point (Schläfli) symbol 6^6 holding the same SBUs and topology as the literature MOF H-$[Mn_6(bta)_8Cl_5]\cdot(H_2O)_4$ ($I\bar{4}2d$ (122)).[30] The two interpenetrated frameworks are stacked on top of each other in *c*-direction with a distance of one unit cell (Figure 1c). The central coordination motif of the structure is a square arrangement of four divalent Mn(2) ions around the central μ_4-Cl(1) anion, which is a well-known MOF SBU for pyrazolates, triazolates and tetrazolates.[26,27] Each of those tetranuclear Mn_4 units is interconnected with four neighboring tetranuclear Mn_4 units by monomeric Mn(1) ions via two μ_2-bridging Cl(2) anions, which are coordinated opposite to the μ_4-Cl(1) (Figure 1). Similar μ_2-chloride bridged Mn^{II} chains are also encountered in the MAF structures built from bistriazolate linkers.[7,8,10,11] All Mn^{II} ions are octahedrally coordinated by two opposing chloride anions and four nitrogen atoms from the eight **ta** ligands coordinated around each tetranuclear Mn_4 unit. Distinct bond distances and angles of the compound are in good agreement with the literature $H[Mn_6(bta)_8Cl_5]\cdot(H_2O)_4$ MOF (Table 2),[30] which also exhibits a distortion of the tetranuclear Mn_4 units observed as perfect squares for all isolated MOF SBUs in literature.[26,27,33] The main differences in **CFA-23** are the Mn(1)-N(3), Mn(2)-N(1) and Mn(2)-N(2) distances, which are each split into two different distances for the corresponding Mn–N pairs of the H-$[Mn_6(\underline{bta})_8Cl_5]\cdot(H_2O)_4$ MOF. Additionally, the four Mn(2) ions showed a smaller out of plane distortion in comparison to the literature structure, which leads to a change of the Mn(1)-Cl(1)-Mn(1) angle for the opposing Mn(1) ions from 165.43(4)° in the literature structure to 171.712(13)° in **CFA-23**. Nearly no differ-

Table 1. Crystal data and structure refinement of **CFA-23**

	CFA-23
Empirical formula	$C_{19}H_{16}Cl_5Mn_6N_{24}O$
Formula	$C_{16}H_{16}Cl_5Mn_6N_{24}\cdot C_3O$
Formula weight/g·mol^{-1}	1103.45
Temperature/K	298(2)
Wavelength/Å	0.71073
Crystal system	Tetragonal
Space group	$P4_2/nnm$
a/Å	a = 14.4426(4)
c/Å	c = 10.2366(3)
Volume/Å^3	2135.24(13)
Z	2
D_g/gcm^{-3}	1.716
μ/mm^{-1}	2.083
F(000)	1082
Crystal size/mm^3	0.08×0.08×0.06
Θ range	2.439 to 27.495°.
Refles collected	29221
Independent reflections	1301 [R(int) = 0.0272]
Completeness	99.7 %
Data/restraints/parameters	1301/4/82
GooF on F^2	1.132
Final R indices [I > 2sigma(I)]	$R_1 = 0.0223$, $wR_2 = 0.0618$
R indices (all data)	$R_1 = 0.0237$, $wR_2 = 0.0626$
Largest diff. peak and hole/e.Å-3	0.407 and −0.389
CCDC No.	2154149

Table 2. Comparison of distinct bond distances [Å] and angles [°] of **CFA-23** with the respective bonds and angles of H-$[Mn_6(bta)_8Cl_5]\cdot(H_2O)_4$

	CFA-23	$H[Mn_6(BTA)_8Cl_5]\cdot(H_2O)_4$
Mn(1)-N(3)	2.2403(14)	2.248(6)/2.242(6)
Mn(1)-Cl(2)	2.5942(6)	2.5313(17)
Mn(2)-N(1)	2.2473(13)	2.270(5)/2.303(5)
Mn(2)-N(2)	2.2266(13)	2.191(6)/2.237(6)
Mn(2)-Cl(1)	2.7028(3)	2.6871(15)
Mn(2)-Cl(2)	2.4888(6)	2.475(2)
Mn(1)-Cl(2)-Mn(2)	92.101(19)	92.02(6)
Mn(2)-Cl(1)-Mn(2) (opposite)	171.712(13)	165.43(4)
Mn(2)-Cl(1)-Mn(2) (neighbouring)	90.299(1)	90.921(5)

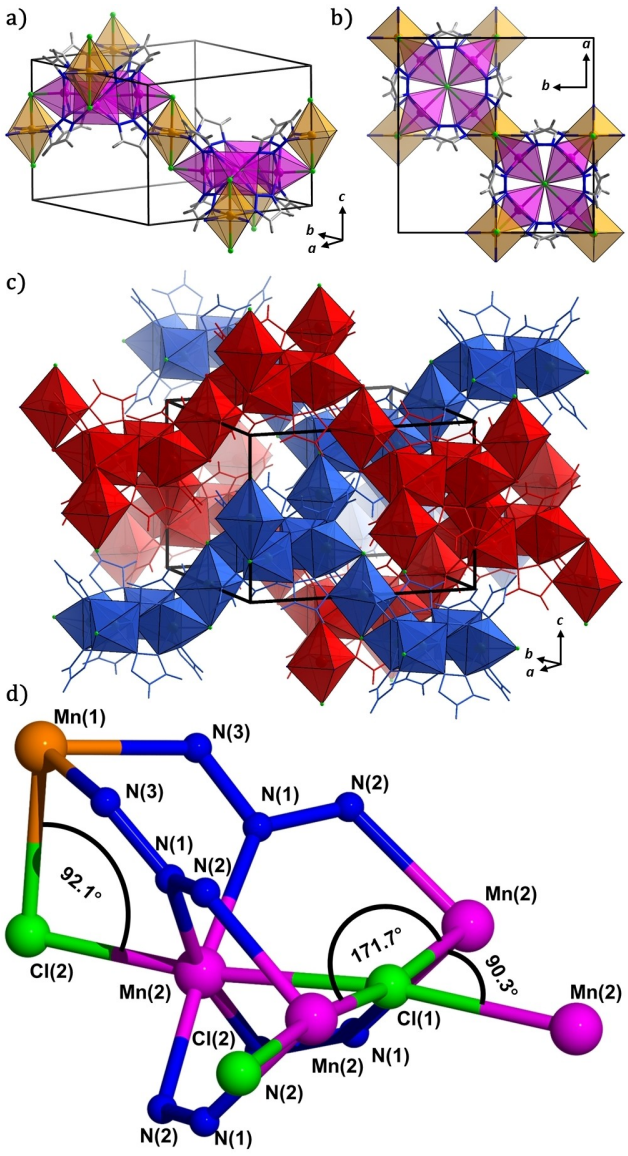

Figure 1. a) Side view and b) view along the *c*-direction visualizing the connection motif of the SBUs in **CFA-23**. c) Visualization of the two interpenetrating frameworks in **CFA-23**. d) Atoms and distinct bond angles of the tetranuclear Mn_4 unit (pink) and the bridging Mn(1) (orange) ions.

ence is observed for the Mn(1)-Cl(2)-Mn(2) angle connecting the Mn_4-tetramers, which indicates a similar spatial arrangement in both frameworks (Figure 1). The resulting negatively charged 3D framework $[Mn_6Cl_5(ta)_8]^-$ has one negative charge per formula unit, which requires charge balancing. The previously reported $H[Mn_6(bta)_8Cl_5]\cdot(H_2O)_4$ compound suggests the presence of a H_3O^+ moiety located at the additional O sites found in the single crystal structure analysis. However, for **CFA-23**, additional electron density was found in small cavities of the structure (Figure S6), indicating a disordered isopropyl alcohol molecule, which is expected to be present as (((propan-2-yl)oxidanium)$^+$ counter ion in the structure. Since the hydrogen atoms could not be refined for this disordered counter-cation, they were added to the sum formula of the structure. Additional proof for this was found via PLATON/SQUEEZE analysis of the structure,[34] which gave a total potential solvent accessible surface area of 557 Å^3 (26% of the 2135.24(13) Å^3 unit cell) with 69 electron counts. Hereof, approximately 31 electron counts are located in each of the two cavities with the counter cations (12.6% of the unit cell volume) and only 4 in each of the two channel pores (13.1% of the unit cell volume) along the *c*-direction of the unit cell (Figure 3, S6). Therefore, indicating accessible and free pore channels in the structure. Further investigations with TGA-MS gave additional evidence for this unusual charge balancing counter ion.

Composition and Thermal Stability

Phase purity of **CFA-23** was confirmed by PXRD, neatly matching the pattern calculated from SC-XRD data (Figure 2a), which was affirmed with a Le Bail fit (Figure S3). In addition, a Mn:Cl ratio of 6:5.1, which is in good agreement with the compound's composition, was obtained by energy dispersive X-ray (EDX) spectroscopy (Figure S11). Optical and SEM micrographs also showed no impurities next to the large crystal specimens (Figure 3, S2). The thermal stability of the compound was investigated by VT-PXRD, revealing a small decrease of crystallinity at temperatures above 350 °C and a nearly complete loss of crystallinity for the pattern at 400 °C (Figure 2b). At temperatures above 400 °C, new reflexes indicate the formation of MnO, although the measurement was conducted under nitrogen gas flow. Hereby, one MnO per formula unit is expected to origin from the(propan-2-yl)oxidanium cations but a contribution from minor leaks in the measurement setup cannot be ruled out. TGA curves also show a decomposition onset in agreement with VT-XRPD patterns. A TGA measurement coupled with mass spectrometry of the decomposition products reveals the loss of small amounts of isopropyl alcohol between 150–270 °C and evolution of propene between 225 to 370 °C (Figure 2c), indicating the decomposition of the (propan-2-yl)oxidanium cations, similar to the decomposition of isopropyl alcohol under acidic conditions.[35] Note here that no trace of acetone (43 m/z), a typical decomposition product of isopropyl alcohol under basic conditions, is observed at the beginning of the decomposition. Thus, affirming the (propan-2-yl)oxidanium cations found in SC-XRD as charge balance for the negatively charged framework.

Porosity

Specific surface areas of 321, 226 and 104 m^2g^{-1} were calculated for H_2, Ar and CO_2, respectively, from the crystal structure of **CFA-23** using the iRaspa software.[36] The 2D pore channels run along the *c*-direction, which can be clearly identified for the obtained single crystals and their morphology (Figure 3). Thus, the separation of gases due to the narrow character of the pores could be a highly interesting field of study. However, no typical adsorption isotherms were observed

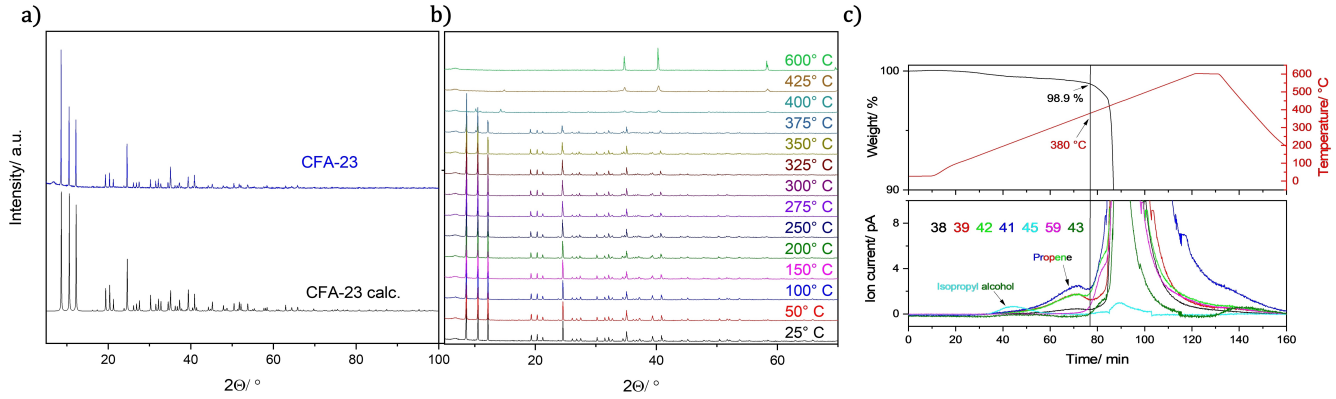

Figure 2. a) Calculated (black), measured (blue) and b) VT-PXRD patterns of **CFA-23**. c) Enlarged TG-curve and simultaneous MS signals of **CFA-23** showing the loss of small quantities of isopropyl alcohol (43 and 45 m/z) between 150–270 °C and evolution of propene (42, 41, 39 and 38 m/z) between 225 to 370 °C, indicating decomposition of the (propan-2-yl)oxidanium cations prior to the framework decomposition

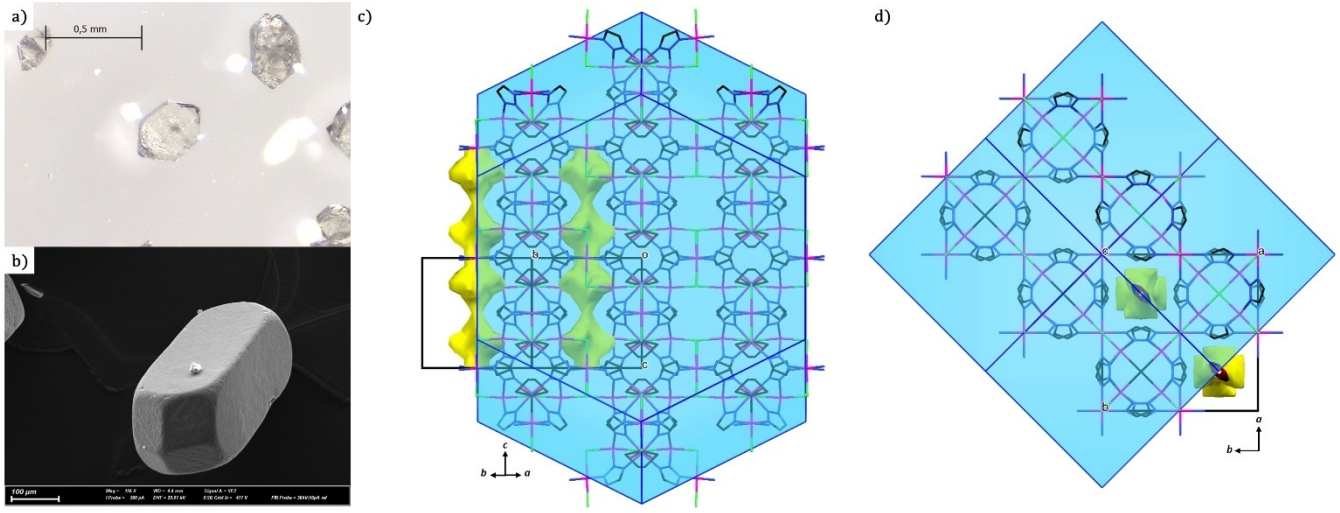

Figure 3. a) Optical and b) SEM micrographs of **CFA-23** and structure plots showing the crystal morphology (blue) and pore channels (yellow) viewed along the c) *ab*- and d) *c*-direction.

for Ar or even H_2 and samples activated at 200 °C so far (Figure S7, S8). This can be explained with the ultra-narrow pore apertures of 2.72 Å (kinetic diameter of H_2 = 2.89 Å) calculated for the **CFA-23** structure using PoreBlazer v4.0.[37] In literature, it is shown that gas molecules such as CO_2 can overcome even narrower pore apertures in MFU-4 (2.22 Å pore limiting diameter calculated with PoreBlazer v4.0) at elevated temperatures and pressures[38] and even kinetic trapping of Xenon and SF_6 is possible.[3,4] However, no adsorption of CO_2 at 273 K for **CFA-23** samples activated at temperatures up to 350 °C (Figure S9) and no kinetic trapping of xenon after 24 h at 30 bar and 100 °C was observed. A possible explanation might be the blockage of the narrow channel pores with residual solvent molecules, displaced (propan-2-yl)oxidanium cations, or other defects, of which only two are necessary to plug a channel. It is also possible that xenon enters the framework without being trapped at ambient conditions and thus already being lost prior to TGA analysis. Nonetheless, the potential porosity of the framework still suggests the classification as a MOF[39] and further kinetic trapping attempts of small molecules at high temperatures and pressures could proof a worthwhile aim.

Magnetization Measurements

The inverse susceptibility $\chi^{-1} = (M/H)^{-1}$ per mol Mn is shown in Figure 4a). Curie-Weiss behavior is observed in the high-temperature region above $T \sim 50$ K. The effective moment amounts to $\mu_{eff} = 6.1\ \mu_B$ per Mn close to the value of 5.92 μ_B expected for free Mn^{2+} ions. The $\chi_M T$ product of **CFA-23** increases monotonously with increasing temperature and reaches a value of 23.22 $cm^3mol^{-1}K$ at $T = 300$ K (Figure S12), which is higher than 19.24 $cm^3mol^{-1}K$ of the literature compound, but still lower than the saturation value of 26.25 $cm^3mol^{-1}K$ expected for 6

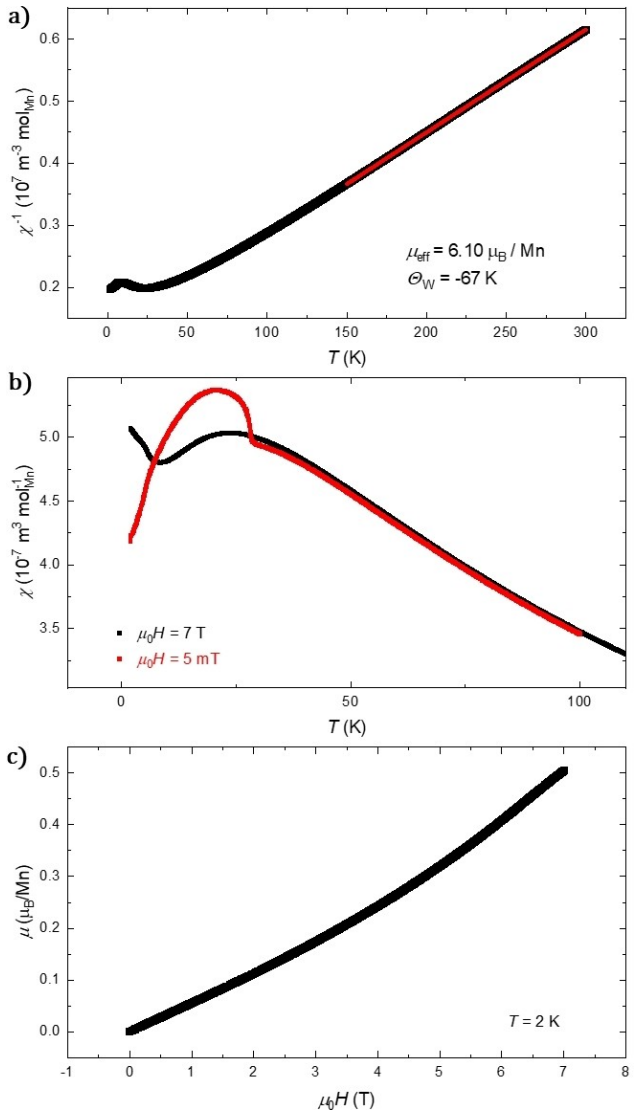

Figure 4. a) Temperature dependence of the inverse molar magnetic susceptibility χ^{-1} in a 7 T field and b) the molar magnetic susceptibility χ in fields of 7 T and 5 mT for **CFA-23** in SI units. c) Isothermal magnetization *M* of **CFA-23** as function of the magnetic field *H* at 2 K.

high-spin d^5 ions with spin-only $g=2.0$ at infinite temperature.[30] This indicates a weaker but still sizeable antiferromagnetic (AFM) exchange in **CFA-23** than found in the literature compound, in agreement with the negative Weiss temperature $\theta_W=-67$ K, as compared to -76 K found for the latter.[30] A small temperature-independent contribution has been considered in the fitting and was found to account for 5% of the room temperature value. Figure 4b) shows χ obtained in applied fields $\mu_0H=5$ mT and 7 T. Only a minute field-dependence is observed for $T>30$ K, in accordance with a magnetically non-ordered state. A sharp increase, which also affirms good crystallinity of the sample and cooperative behavior of the transition, takes place in small applied fields of 5 mT when cooling below $T=28.5$ K. In contrast, the increase for the literature compound already starts at $T=46$ K in a 100 mT field. This behavior, together with the decrease in χ upon further cooling, indicates a canted AFM ordering with a complex interplay of temperature-dependent exchange, tilting angle, and/or steric effects. The anomaly is shifted to lower temperature in larger applied fields, consistent with AFM ordering. Comparison of the resulting frustration parameters of $f=2.4$ for **CFA-23** and $f=1.7$ for $H[Mn_6(bta)_8Cl_5]\cdot(H_2O)_4$, indicates a slight increase in frustration for **CFA-23**. Isothermal magnetization at $T=2$ K is plotted in Figure 4c). The magnetization does not approach saturation even in the largest applied field of $\mu_0H=7$ T in accordance with the proposed AFM ordering. A weak increase in slope, not observed for the literature counterpart, is found at $\mu_0H\sim5$ T, which could indicate the onset of a broad metamagnetic transition. In order to gain a deeper insight into the magnetic behavior of the materials two different methods were applied to fit the susceptibility of the material. In a first approach the numerical expression derived by Rushbrooke and Wood[40] for a basic antiferromagnetic quadratic lattice with exchange coupling J_1, was applied.[41] Hereby, with a J_1 value of -4.1 K the high-temperature behavior matched the experimental data but a slight shift of the maximum to a higher temperature of 35 K was obtained in comparison to $T_{max}=24$ K observed in the experiment (Figure 5c). Thus, the molar susceptibility was also fitted using a molecular approach with the program PHI,[42] similar to the method reported previously,[43] which adds the J_2 coupling to the model. This molecular model resulted in an improved match of the high-temperature behavior, as well as a shift of the maximum to 30 K closer to the experimental results (Figure 5c). Hereby, the value of the main exchange parameter did not change with -4.1 K, but is now assigned to J_2, whereas J_1 decreased to -0.37 K. The two antiferromagnetic couplings suggest frustration of tetranuclear Mn_4 unit. This tetranuclear Mn_4 unit seems to be sufficient for a reasonable approximation of the susceptibility since the bridging Mn^{II} ions are considered to contribute mainly as mediator between the tetranuclear Mn_4 units, because the nature of the J_3 coupling has no influence on the spin-orientation of the neighboring tetramer.Taking J_3 into our model would go beyond simple approaches. Simulation of the isothermal magnetization *M* as function of the magnetic field *H* at 2 K applying the obtained exchange coupling constants for the molecular model reproduces the experimentally observed curvature, although the results should be regarded with caution due to the field dependent phase transition already occurring at higher temperatures. In conclusion, the small differences in bond lengths and angles of the structures are expected to be responsible for the change in magnetic behavior in comparison to the literature compound, although effects from the interactions between the two interpenetrating frameworks, as well as the differing counter anions and residual solvents, cannot be ruled out. Thus, investigation of analogous structures, as well as more detailed computational simulations, are necessary in order to derive trends for the structure-magnetism relation, which could be applied to predict and design enhanced magnetic properties into new materials.

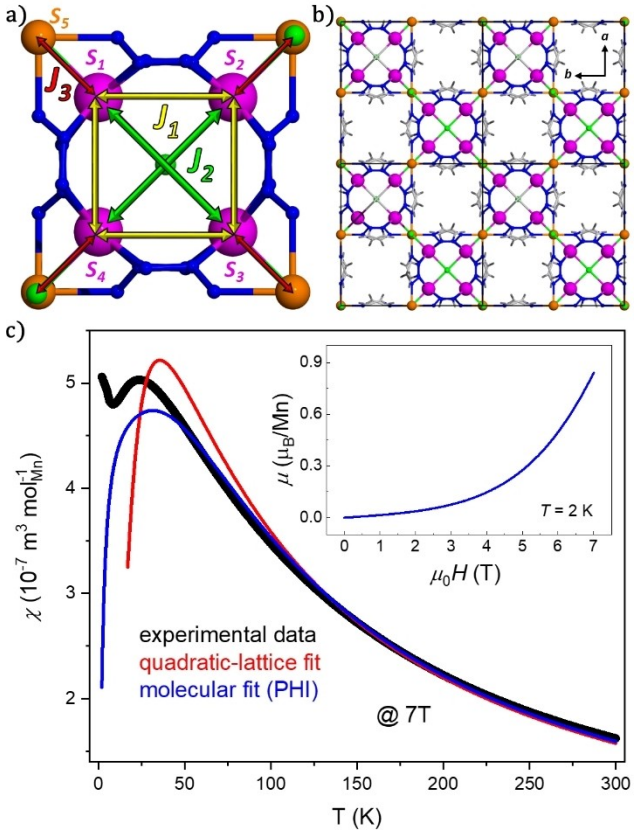

Figure 5. a) Mn^{II}-Mn^{II} exchange couplings J_1 (yellow), J_2 (green) and J_3 (red) in the basic Mn_4-tetramer (pink) and the bridging Mn^{II} ions (orange) of **CFA-23**. b) Ball-and-stick view along the *c*-direction of one of the interpenetrating **CFA-23** nets showing the linkage mode of the Mn_4-tetramers. c) Measured magnetic susceptibility χ in a 7 T field per Mn^{II} ion in comparison to the fits obtained from the quadratic-layer and molecular models. The inset shows the isothermal magnetization *M* as function of the magnetic field *H* at 2 K calculated from the exchange coupling constants obtained from the molecular fit.

Conclusions

In summary, the novel **CFA-23** coordination framework was prepared from the **H-ta** ligand and $MnCl_2 \cdot 4H_2O$ under solvothermal conditions and the structure solved using SC-XRD, revealing a two-fold interpenetration of frameworks with the same topology as the literature-known spin-canted MOF H-$[Mn_6(bta)_8Cl_5] \cdot (H_2O)_4$.[30] The compound was further characterized by FT-IR, XRPD, TGA, TGA-MS and VT-XRPD. In contrast to the literature structure, **CFA-23** features a two-fold interpenetration and pore channels along the *c*-direction, which is presumably due to the absence of the steric crowding effect of the benzene ring at the H-bta ligand. In contrast to isolated tetranuclear Mn_4 units observed in some literature MOFs, spin-coupling and long-range order throughout the frameworks is observed due to the linking of the secondary building units via bridging Mn^{II} sites. However, the tetrameric unit seems to be the main contributor for the magnetic behavior, as the susceptibility and magnetization can be already reasonably fitted with two exchange-couplings, indicating only a mediating magnetic function of the Mn^{II} bridges. In addition, the magnetic measurements revealed a differing behavior in comparison to the literature counterpart, which indicates that minute lattice distortions due to sterically demanding ligands or framework interpenetration strongly influence the magnetic properties in such frameworks. Thus, although minor contributions from the counter cations or residual solvent molecules should not be neglected, we conclude that fine tuning and tailoring of magnetic properties might be achieved with ligands exhibiting varying steric demands, which is currently under investigation.

Experimental Section

Materials and General Methods

Isopropyl alcohol (≥ 99.8 %, VWR), $MnCl_2 \cdot 4H_2O$ (99.99 %, abcr), and **H-ta** (98 %; BLD Pharmatech Ltd.) were used as obtained from the commercial supplier. A general purpose acid digestion vessel (Parr Instrument Company) with 23 mL inner volume teflon liners was used for the solvothermal reaction.

Attenuated total reflectance (ATR) Fourier transform infrared spectroscopy (FT-IR) in the range of 4000–400 cm^{-1} was measured with the PLATINUM ATR unit and a KBr (4000-400 cm^{-1}) beam splitter on a Bruker Equinox 55 FT-IR spectrometer. The signals were labelled strong (s), medium (m) and weak (w). SEM micrographs were recorded with a Philips XL 30 FEG scanning electron microscope and a Zeiss Crossbeam 550, which was also used for EDX spectra of carbon coated samples using the analytical silicon drift detector from Oxford Instruments. An Empyrean (PANalytical) diffractometer equipped with Bragg-Brentano^{HD} mirror and PIXcel^{3D} 2×2 detector was used to collect the PXRD and VT-PXRD pattern using the XRK 900 reactor chamber. The sample was heated with a rate of 5 °C min^{-1} with a 30 min isothermal step prior to measurement under nitrogen atmosphere. The pattern at 25 °C was measured in the range of 5–100° 2θ with 0.0131° steps and an overall measurement time of 6017 s. All other patterns were collected in the range from 5–70° 2θ with 0.0263° steps and a measurement time of 2127 s for each pattern. Thermogravimetric analysis (TGA) was conducted with a heating rate of 5 °C min^{-1} and starting after a five-minute isothermal step on a TA Instruments Q500 device in the temperature range of 25–800 °C under nitrogen gas flow. A Netzsch STA 409 C thermobalance connected via Skimmer coupling to a Balzers QMG 421 mass spectrometer was used for the TGA-MS analysis in the temperature range from 25–600 °C and a 5 °C min^{-1} heating rate under nitrogen atmosphere. The argon adsorption isotherm was measured on a Quantachrome Autosorb-I ASI-CP-8 instrument at 77.3 K in the range of $5.00 \times 10^{-5} \leq p/p_0 \leq 1.00$. The H_2 adsorption experiment at 50 K was conducted with a BELSORP-max instrument combined with a BELCryo system. The samples were treated at 200 °C in high vacuum for several hours prior to the measurements. CO_2 adsorption measurements were performed on a Quantachrome NOVA2000 Series instrument at 273 K after vacuum treatment at 200 °C, 300 °C, and 350 °C for 2 h. Temperature- and field-dependent magnetization was measured using a Quantum Design MPMS3. The powder sample with a total mass of m = 7.43 mg was mounted in a plastic capsule.

Single-crystal X-ray Data Collection and Structure Refinement

X-ray diffraction data for the single crystal structure determination were collected at room temperature on a Bruker D8 Venture diffractometer (Mo Kα radiation, λ = 0.71073 Å). The raw data frames were integrated and corrected for absorption effects using the Bruker SAINT[44] and SADABS[45] software packages. Structure solution by direct methods and structure refinement by full-matrix least-squares techniques against F2 were performed using SHELXT 2014/5[46] and SHELXL 2018/3.[47] All non-hydrogen atoms of the framework were refined anisotropically and the positions of framework hydrogen atoms were determined from the difference Fourier map. The atomic coordinates of protonated isopropanol, which is disordered due to the symmetry over four positions, were refined by means of the DSR program.[48] The occupancies of the atoms were set at 0.25. Because of highly disordered solvent, the hydrogen atoms in protonated isopropanol were omitted in the refinement. Complete crystallographic data for the **CFA-23** structure reported in this paper have been deposited in the CIF format in the Cambridge Crystallographic Data Center as supplementary publication no. 2154149.

Synthesis of CFA-23 (((propan-2-yl)oxidanium)$^{+}$[$Mn_6Cl_5(ta)_8$]$^{-}$)

$MnCl_2 \cdot 4H_2O$ (49.5 mg, 0.250 mmol) was dissolved in 5 mL of isopropyl alcohol inside of a new 23 mL teflon liner in an ultrasonic bath. H-ta (34.6 mg, 0.500 mmol) was added, the reaction mixture sealed in the digestion vessel and heated in an oven at 210 °C for 3 days employing a heating and cooling rate of 1 °C/min. The product was obtained after filtration and washing with 5 mL of isopropyl alcohol as large colourless crystals, which were dried under vacuum for several hours (37.5 mg, 82 %). FT-IR (ATR, 4000–400 cm^{-1}): 3142 (w), 3125 (w), 1745 (w), 1607 (w), 1478 (w), 1451 (m), 1419 (m), 1380 (w), 1206 (w), 1177 (s), 1096 (s), 993 (m), 972 (s), 881 (w), 812 (s), 797 (s), 712 (m). EDX Mn : Cl ratio: 6 : 5.1.

Acknowledgements

Financial support from the DFG (SPP 1928 COORNETs: Coordination Networks: Building Blocks for Functional Systems) is gratefully acknowledged. H.-A. K.v.N. acknowledges funding by DFG within TRR 80 "From Electronic Correlations to Functionality", project no. 107745057 (Augsburg, Munich, Stuttgart) Open Access funding enabled and organized by Projekt DEAL.

Conflict of Interest

The authors declare no conflict of interest.

Data Availability Statement

The data that support the findings of this study are available from the corresponding author upon reasonable request.

Keywords: coordination framework · metal-organic framework · magnetic properties · manganese · microporous materials

[1] R. Ettlinger, M. Sönksen, M. Graf, N. Moreno, D. Denysenko, D. Volkmer, K. Kerl, H. Bunzen, *J. Mater. Chem. B* **2018**, *6*, 6481–6489.
[2] a) D. Denysenko, T. Werner, M. Grzywa, A. Puls, V. Hagen, G. Eickerling, J. Jelic, K. Reuter, D. Volkmer, *Chem. Commun.* **2012**, *48*, 1236–1238; b) D. Denysenko, J. Jelic, K. Reuter, D. Volkmer, *Chem. Eur. J.* **2015**, *21*, 8188–8199; c) D. Denysenko, J. Jelic, O. V. Magdysyuk, K. Reuter, D. Volkmer, *Microporous Mesoporous Mater.* **2015**, *216*, 146–150; d) D. Denysenko, M. Grzywa, J. Jelic, K. Reuter, D. Volkmer, *Angew. Chem.* **2014**, *126*, 5942–5946; e) D. Denysenko, D. Volkmer, *Faraday Discuss.* **2017**, *201*, 101–112; f) R. J. Comito, K. J. Fritzsching, B. J. Sundell, K. Schmidt-Rohr, M. Dincă, *J. Am. Chem. Soc.* **2016**, *138*, 10232–10237; g) E. D. Metzger, R. J. Comito, Z. Wu, G. Zhang, R. C. Dubey, W. Xu, J. T. Miller, M. Dincă, *ACS Sustainable Chem. Eng.* **2019**, *7*, 6654–6661; h) E. D. Metzger, R. J. Comito, C. H. Hendon, M. Dincă, *J. Am. Chem. Soc.* **2017**, *139*, 757–762; i) A. M. Wright, C. Sun, M. Dincă, *J. Am. Chem. Soc.* **2021**, *143*, 681–686.
[3] H. Bunzen, F. Kolbe, A. Kalytta-Mewes, G. Sastre, E. Brunner, D. Volkmer, *J. Am. Chem. Soc.* **2018**, *140*, 10191–10197.
[4] H. Bunzen, A. Kalytta-Mewes, L. van Wüllen, D. Volkmer, *Beilstein J. Nanotechnol.* **2019**, *10*, 1851–1859.
[5] a) J. Teufel, H. Oh, M. Hirscher, M. Wahiduzzaman, L. Zhechkov, A. Kuc, T. Heine, D. Denysenko, D. Volkmer, *Adv. Mater.* **2013**, *25*, 635–639; b) I. Weinrauch, I. Savchenko, D. Denysenko, S. M. Souliou, H.-H. Kim, M. Le Tacon, L. L. Daemen, Y. Cheng, A. Mavrandonakis, A. J. Ramirez-Cuesta, D. Volkmer, G. Schütz, M. Hirscher, T. Heine, *Nat. Commun.* **2017**, *8*, 14496.
[6] a) R. Röß-Ohlenroth, B. Bredenkötter, D. Volkmer, *Organometallics* **2019**, *38*, 3444–3452; b) C. Jin, S. Zhang, Z. Zhang, Y. Chen, *Inorg. Chem.* **2018**, *57*, 2169–2174; c) Z. Cai, C. E. Bien, Q. Liu, C. R. Wade, *Chem. Mater.* **2020**, *32*, 4257–4264; d) C. E. Bien, Q. Liu, C. R. Wade, *Chem. Mater.* **2020**, *32*, 489–497; e) A. M. Wright, Z. Wu, G. Zhang, J. L. Mancuso, R. J. Comito, R. W. Day, C. H. Hendon, J. T. Miller, M. Dincă, *Chem* **2018**, *4*, 2894–2901.
[7] P.-Q. Liao, X.-Y. Li, J. Bai, C.-T. He, D.-D. Zhou, W.-X. Zhang, J.-P. Zhang, X.-M. Chen, *Chem. Eur. J.* **2014**, *20*, 11303–11307.
[8] A. J. Rieth, Y. Tulchinsky, M. Dincă, *J. Am. Chem. Soc.* **2016**, *138*, 9401–9404.
[9] J. J. Oppenheim, J. L. Mancuso, A. M. Wright, A. J. Rieth, C. H. Hendon, M. Dincaˇ, *J. Am. Chem. Soc.* **2021**, *143*, 16343–16347.
[10] P.-Q. Liao, H. Chen, D.-D. Zhou, S.-Y. Liu, C.-T. He, Z. Rui, H. Ji, J.-P. Zhang, X.-M. Chen, *Energy Environ. Sci.* **2015**, *8*, 1011–1016.
[11] K. Knippen, B. Bredenkötter, L. Kanschat, M. Kraft, T. Vermeyen, W. Herrebout, K. Sugimoto, P. Bultinck, D. Volkmer, *Dalton Trans.* **2020**, 15758–15768.
[12] H. Bunzen, M. Grzywa, R. Aljohani, H.-A. Krug von Nidda, D. Volkmer, *Eur. J. Inorg. Chem.* **2019**, *2019*, 4471–4476.
[13] L. Sun, C. H. Hendon, S. S. Park, Y. Tulchinsky, R. Wan, F. Wang, A. Walsh, M. Dincă, *Chem. Sci.* **2017**, *8*, 4450–4457.
[14] H. Bunzen, A. Javed, D. Klawinski, A. Lamp, M. Grzywa, A. Kalytta-Mewes, M. Tiemann, H.-A. K. von Nidda, T. Wagner, D. Volkmer, *ACS Appl. Nano Mater.* **2019**, *2*, 291–298.
[15] S. Biswas, M. Tonigold, M. Speldrich, P. Kögerler, M. Weil, D. Volkmer, *Inorg. Chem.* **2010**, *49*, 7424–7434.
[16] K. Knippen, D. Matuszczyk, M. Kraft, B. Bredenkötter, G. Eickerling, T. Lis, D. Volkmer, M. Stępień, *Chem. Eur. J.* **2021**.
[17] R. Röß-Ohlenroth, C. Freudig, M. Kraft, H. Bunzen, D. Volkmer, *Cryst. Growth Des.* **2022**, *22*, 379–391.
[18] F. Gándara, F. J. Uribe-Romo, D. K. Britt, H. Furukawa, L. Lei, R. Cheng, X. Duan, M. O'Keeffe, O. M. Yaghi, *Chem. Eur. J.* **2012**, *18*, 10595–10601.

[19] M. Grzywa, D. Denysenko, J. Hanss, E.-W. Scheidt, W. Scherer, M. Weil, D. Volkmer, *Dalton Trans.* **2012**, *41*, 4239–4248.
[20] X.-H. Zhou, Y.-H. Peng, X.-D. Du, J.-L. Zuo, X.-Z. You, *CrystEngComm* **2009**, *11*, 1964.
[21] a) M. Grzywa, R. Röß-Ohlenroth, C. Muschielok, H. Oberhofer, A. Błachowski, J. Żukrowski, D. Vieweg, H.-A. K. von Nidda, D. Volkmer, *Inorg. Chem.* **2020**, *59*, 10501–10511; b) A. B. Andreeva, K. N. Le, K. Kadota, S. Horike, C. H. Hendon, C. K. Brozek, *Chem. Mater.* **2021**, *33*, 8534–8545.
[22] J. G. Park, M. L. Aubrey, J. Oktawiec, K. Chakarawet, L. E. Darago, F. Grandjean, G. J. Long, J. R. Long, *J. Am. Chem. Soc.* **2018**, *140*, 8526–8534.
[23] J. G. Park, B. A. Collins, L. E. Darago, T. Runčevski, M. E. Ziebel, M. L. Aubrey, H. Z. H. Jiang, E. Velasquez, M. A. Green, J. D. Goodpaster, J. R. Long, *Nat. Chem.* **2021**, *13*, 594–598.
[24] R. Nutakki, R. Röß-Ohlenroth, D. Volkmer, A. Jesche, H.-A. K. von Nidda, A. A. Tsirlin, P. Gegenwart, L. Pollet, L. D. C. Jaubert, *arXiv.org* **2022**, 2203.08780v1.
[25] a) Z. Guo, D. Yan, H. Wang, D. Tesfagaber, X. Li, Y. Chen, W. Huang, B. Chen, *Inorg. Chem.* **2015**, *54*, 200–204; b) C. K. Brozek, A. F. Cozzolino, S. J. Teat, Y.-S. Chen, M. Dincă, *Chem. Mater.* **2013**, *25*, 2998–3002.
[26] M. Dincă, A. Dailly, Y. Liu, C. M. Brown, D. A. Neumann, J. R. Long, *J. Am. Chem. Soc.* **2006**, *128*, 16876–16883.
[27] D. J. Xiao, M. I. Gonzalez, L. E. Darago, K. D. Vogiatzis, E. Haldoupis, L. Gagliardi, J. R. Long, *J. Am. Chem. Soc.* **2016**, *138*, 7161–7170.
[28] R. Poloni, K. Lee, R. F. Berger, B. Smit, J. B. Neaton, *J. Phys. Chem. Lett.* **2014**, *5*, 861–865.
[29] G. Mínguez Espallargas, E. Coronado, *Chem. Soc. Rev.* **2018**, *47*, 533–557.
[30] S.-D. Han, J.-P. Zhao, Y.-Q. Chen, S.-J. Liu, X.-H. Miao, T.-L. Hu, X.-H. Bu, *Cryst. Growth Des.* **2014**, *14*, 2–5.
[31] C.-T. He, Z.-M. Ye, Y.-T. Xu, D.-D. Zhou, H.-L. Zhou, Da Chen, J.-P. Zhang, X.-M. Chen, *Chem. Sci.* **2017**, *8*, 7560–7565.
[32] V. A. Blatov, A. P. Shevchenko, D. M. Proserpio, *Cryst. Growth Des.* **2014**, *14*, 3576–3586.
[33] a) D. Chen, W. Shi, P. Cheng, *Chem. Commun.* **2015**, *51*, 370–372; b) M. Asgari, S. Jawahery, E. D. Bloch, M. R. Hudson, R. Flacau, B. Vlaisavljevich, J. R. Long, C. M. Brown, W. L. Queen, *Chem. Sci.* **2018**, *9*, 4579–4588; c) S. Biswas, M. Maes, A. Dhakshinamoorthy, M. Feyand, D. E. de Vos, H. Garcia, N. Stock, *J. Mater. Chem.* **2012**, *22*, 10200; d) J.-H. Liao, W.-T. Chen, C.-S. Tsai, C.-C. Wang, *CrystEngComm* **2013**, *15*, 3377; e) K. Sumida, S. Horike, S. S. Kaye, Z. R. Herm, W. L. Queen, C. M. Brown, F. Grandjean, G. J. Long, A. Dailly, J. R. Long, *Chem. Sci.* **2010**, *1*, 184.
[34] A. L. Spek, *Acta Crystallogr. Sect. D* **2009**, *65*, 148–155.
[35] L. Silvester, J.-F. Lamonier, C. Lamonier, M. Capron, R.-N. Vannier, A.-S. Mamede, F. Dumeignil, *ChemCatChem* **2017**, *9*, 2250–2261.
[36] D. Dubbeldam, S. Calero, T. J. Vlugt, *Mol. Simul.* **2018**, *44*, 653–676.
[37] L. Sarkisov, R. Bueno-Perez, M. Sutharson, D. Fairen-Jimenez, *Chem. Mater.* **2020**, *32*, 9849–9867.
[38] G. Sastre, J. van den Bergh, F. Kapteijn, D. Denysenko, D. Volkmer, *Dalton Trans.* **2014**, *43*, 9612–9619.
[39] S. R. Batten, N. R. Champness, X.-M. Chen, J. Garcia-Martinez, S. Kitagawa, L. Öhrström, M. O'Keeffe, M. Paik Suh, J. Reedijk, *Pure Appl. Chem.* **2013**, *85*, 1715–1724.
[40] G. S. Rushbrooke, P. J. Wood, *Mol. Phys.* **1958**, *1*, 257–283.
[41] M. E. Lines, *J. Phys. Chem. Solids* **1970**, *31*, 101–116.
[42] N. F. Chilton, R. P. Anderson, L. D. Turner, A. Soncini, K. S. Murray, *J. Comb. Chem.* **2013**, *34*, 1164–1175.
[43] T. W. Werner, S. Reschke, H. Bunzen, H.-A. K. von Nidda, J. Deisenhofer, A. Loidl, D. Volkmer, *Inorg. Chem.* **2016**, *55*, 1053–1060.
[44] SAINT; Bruker Analytical X-Ray Systems, Inc., Madison, WI, **2015**..
[45] L. Krause, R. Herbst-Irmer, G. M. Sheldrick, D. Stalke, *J. Appl. Crystallogr.* **2015**, *48*, 3–10.
[46] G. M. Sheldrick, *Acta Crystallogr. Sect. A* **2015**, *71*, 3–8.
[47] G. M. Sheldrick, *Acta Crystallogr. Sect. C* **2015**, *71*, 3–8.
[48] D. Kratzert, I. Krossing, *J. Appl. Crystallogr.* **2018**, *51*, 928–934.

Manuscript received: April 16, 2022
Revised manuscript received: June 8, 2022
Accepted manuscript online: June 17, 2022

